Fourier Transform Rheology of Branched Polyethylene: Experiments and Models for Assessing the Macromolecular Architecture

Guy Schlatter,* Guillaume Fleury, and René Muller

Laboratoire d'Ingénierie des Polymères pour les Hautes Technologies (LIPHT), FRE 2711, Ecole Européenne de Chimie Polymères et Matériaux de Strasbourg (ECPM), 25 Rue Becquerel, 67087 Strasbourg Cedex 2, France

Received March 15, 2005; Revised Manuscript Received May 20, 2005

ABSTRACT: Fourier transform rheology (FTR) consists of analyzing the frequency spectrum of the nonlinear torque response obtained during large-amplitude oscillatory shear. In the present work, the analysis has been carried out in the whole complex space and was especially focused on the study of the third complex harmonic I^*_3/I_1 ($= I^*(3\omega_1)/I_1$, where I_1 is the spectrum intensity at the fundamental frequency ω_1), the intensity I_3/I_1 ($= |I^*_3/I_1|$), and the phase shift Φ_3 of I^*_3/I_1. The accuracy of FTR to characterize the architecture of linear, sparsely, and densely branched polyethylene regarding the number of branches and their length has been shown. A modified Wagner integral model and a differential multimode pompom model were used to simulate FTR experiments. Nonlinear parameters of each model were determined by fitting the curve of the third complex harmonic I^*_3/I_1 versus the strain amplitude γ_0 with the experimental data. Good results have been obtained with the modified Wagner model. Whereas, the pompom model accounts for the experimental intensity of the third harmonic, discrepancies remain for the phase shift behavior Φ_3 for the polymers showing the highest nonlinear behavior regarding the level of I_3/I_1. Nevertheless, when fitting was possible, the results have been correlated with the supposed structure expected from the type of synthesis.

1. Introduction

The characterization of molecular structure of long-chain branching (LCB) is a crucial point of research. It is well-known that branching architecture significantly affects the rheological properties of molten branched polymers. Thus, LCB increases the viscosity, involves the onset of shear thinning at a much lower shear rate, and is the cause of strain-hardening in elongation. However, it is difficult to differentiate the effects of each molecular structural characteristic (such as molecular weight and its distribution, number of branches and their length, etc.) on rheological properties. There is no unique tool, but the combination of several significant experimental methods and their models should be able to provide information for assessing LCB.

Fujimoto et al.,[1] then Roovers,[2] and more recentl,y Daniels et al.[3] have experimentally studied the rheology of well-defined comb polymers. The authors have shown long-time relaxation processes that are not present for linear polymers. Typically, the arms provide a star behavior at high frequencies, whereas the terminal relaxation at lower frequencies is related to the cross-bar reptation. To characterize linear and nonlinear viscoelastic behaviors, specific constitutive phenomenological models have been developed. The single-integral K-BKZ model (Kaye,[4] Bernstein et al.,[5] Wagner and Laun[6]) has proven its efficiency to predict typical behavior of branched polymers. For example, a K-BKZ model is able to fit strain-softening in shear as much as strain-hardening in uniaxial elongation (Wagner et al.[7]). To decrease computational complexity for 2D and 3D flow geometries, multimode differential viscoelastic models have been developed (Baaijens et al.,[8] Béraudo et al.[9]). Although these models are able to quantitatively predict experimental observations, it is difficult to associate physical interpretations in a macromolecular sense. The pompom constitutive model built thanks to tube-based molecular theory (McLeish and Larson,[10] McLeish et al.,[11] Inkson et al.,[12] Read and McLeish,[13] Blackwell et al.,[14] and Groves et al.[15]) is a new tool allowing understanding of rheological phenomena in the light of macromolecular behavior. In particular, these authors have studied both theoretically and experimentally the rheology of well-controlled H-shaped and branched polymer melts. They have measured and simulated G' and G'' for well-defined H-shaped polymers in a wide range of frequencies. They have clearly explained the typical two-peak shape of the $G''(\omega)$ plot. They have shown that the peak at high frequencies is allotted to the relaxation of the arms of H-shaped polymers. On the other hand, the authors have shown that increasing the length of the backbone (i.e., increasing the number of entanglement units) shifts the second peak to lower frequencies. The linear dynamics of H-shaped polymers can be characterized by retraction (contraction of the chain within the tube) of dangling arms at short times then by reptation/fluctuation (global displacement by diffusion of the chain) of the backbone at long times. Furthermore, they also have shown that polydispersity in the arm molecular weight drastically shifts the retraction phenomenon to long relaxation times. Vega et al.[16] and Yan et al.[17] have studied the rheological properties of different branched polymers that were beforehand characterized by SEC and ^{13}C NMR respectively. The authors have shown significant effects of LCB density on the shear thinning effect. For the same molecular weight and within a low LCB window, higher LCB density leads to higher viscosity at low shear rates and lower viscosity at high shear rates. However, by studying monodisperse polymers for a wide range of branch content, Janzen and Colby[18] have clearly shown that the relationship between zero-shear viscosity and LCB density is nonmonotonic. Indeed, for a given molecular weight, the zero-shear viscosity increases with LCB density until an upper

10.1021/ma0505530 CCC: $30.25
Published on Web 06/29/2005

bond, then decreases for the highest LCB, which corresponds to low polymer hydrodynamic volumes. Vega et al.[16] have tested 13 metallocene-catalyzed polyethylenes (PEs). By plotting the $\eta'-\eta''$ Cole−Cole diagram, the authors have determined η_0, the limiting extrapolated viscosity and λ_c, the characteristic relaxation time corresponding to the frequency when the function η'' is maximum. After plotting λ_c versus M_w and η_0 versus M_w, three groups of polyethylene samples clearly appear, one group corresponding to linear samples and two groups corresponding to the branched polyethylene. The two latter groups have been allotted to long-chain branched polymers that differ in the amount of branches. Vega et al.[16] reported also the results of the activation energy versus ν (degree of hexyl branching per 1000 carbon atoms). Once more, the group of linear polymers differs from the other two groups of branched polymers that have higher flow-activation energy. These results confirm those presented by Malmberg et al.[19,20] and Baird et al.[21] Unfortunately, this method is not able to differentiate the two groups of branched polymers. An original way to analyze the LCB effect by linear dynamical measurements has been proposed by Trinkle et al.[22,23] It consists of analyzing the rheological experiments by plotting the loss angle δ ($= \tan^{-1}[G''/G']$) versus a reduced modulus G_{red}, defined as the magnitude of the complex modulus divided by the plateau modulus G_N^0 (obtained when $\delta \rightarrow 0$). This technique, the so-called van Gurp−Palmen analysis (van Gurp and Palmen[24]) allows the highlighting of structural effects, like molecular weight distribution and LCB, on rheological properties while minimizing the molecular weight effect. Furthermore, the authors have built a map plotted from characteristic points $P_c(G_{red,c}, \delta_c)$, on which typical branched polymer structures cover distinct areas. Vega et al.,[16] Garcia-Franco et al.,[25] then Lohse et al.[26] also have used this methodology to analyze well-defined long-chain branched polyethylene. Particularly, by using the experimental data of Wood-Adams et al.,[27] Garcia-Franco et al.[25] have explained that branching exhibited physical gellike behavior near the critical gelation point. More recently, Robertson et al.[28] have quantified the extent of LCB by measuring the loss angle peak δ_c within the frequency window where the molten polymer has a physical gel behavior. After assuming that their studied polymer can be considered as a blend of linear and branched macromolecules, the authors have shown that the weight fraction of branched species is linearly correlated with the level of δ_c.

Rheology in the nonlinear domain (high strains) has also been investigated to characterize LCB. McLeish et al.[11] and Heinrich et al.[29] have experimentally and theoretically (by using the pompom model) studied the dynamics of H-shaped polymers during step−strain experiments and have confirmed their results by means of small-angle neutron scattering SANS. The authors have shown the effect of the rearrangement of the branches on SANS that corresponds to a characteristic relaxation time allotted to the stretch of the "cross-bar" of the H-shaped polymers. Doerpinghaus and Baird[30] have used a multimode differential pompom constitutive model to predict shear and extensional experiments. By fitting the parameters of the model, the authors were able to assess LCB of sparsely branched polyethylenes. Another way to characterize LCB should be nonlinear dynamical oscillatory rheology (Fourier transform rheology, FTR), which consists of analyzing the response in the Fourier space. MacSporran and Spiers[31,32] and, more recently, Hyun et al.[33] have studied the nonlinear response for complex fluids in solution. The authors have shown that large-amplitude oscillatory shear is sensitive to the microstructure of the studied fluids. Wilhelm et al.[34−36] have studied the nonlinear dynamical response for different well-defined linear polymers. They have particularly correlated the relative intensity of the third harmonic as a function of the shear amplitude with the molar mass of the tested polymer. Leblanc[37] has shown the capability of FTR to be a sensitive technique for rubber characterization. Debbaut and Buhrin,[38] then Clemeur et al.[39] have characterized polyethylene thanks to large-amplitude oscillatory shear experiments. Clemeur et al.[39] have shown that a differential multimode pompom equation seems to be suitable to model such experiments.

In a previous paper (Fleury et al.[40]), we have compared and correlated different rheological methods to characterize the LCB. The present work focuses on FTR methodology. Moreover, the polymers have been tested in a wider scale of frequencies and an analysis in the complex space of the Fourier transform of the dynamical response will be presented theoretically and experimentally. We have investigated the behavior of nine molten polyethylenes (two linear and seven densely and sparsely branched) thanks to Fourier transform rheology. A K-BKZ integral model and a differential multimode pompom model have been compared to the experiments. The model parameters have been fitted for each polymer in order to discuss their macromolecular structure.

2. Experimental Section

2.1. Materials. A wide variety of polyethylenes have been used to perform these experiments. They were synthesized in the Atofina laboratory (Feluy, Belgium). SEC characterization has been carried out at Atofina laboratory and at the Max Planck Institute (Mainz, Germany). Samples were dissolved in TCB at 140 °C. Unfortunately, both at Atofina laboratory and at MPI, SEC on BR1 was not possible because of the huge difficulty to dissolve it. Table 1 presents the supposed chain structure and SEC results (molecular weights and polydispersity) of the studied polymers.

We disposed of nine different products with a large range of polydispersity but with molecular weight M_w at the same order. LM1 and BM1−BM6 are polyethylenes synthesized by chrome−metallocene catalysis. LM2 is polyethylene synthesized by the Ziegler−Natta technique, while BR1 has been performed by radical synthesis. LM1 is a linear polyethylene with a low degree of polydispersity, while LM2 is linear but has a broader polydispersity. Moreover, thanks to the Ziegler−Natta catalyst, LM2 does not have long-chain branching (Hamielec and Soares[41]). BM1−BM6 are branched polyethylenes including long-chain branching. BR1 is a polyethylene with many short and long branches. All samples have been stabilized by antioxidants during the commercial pelletization operations.

2.2. Rheological Measurements. Equipment. Our experimental setup is based on a Rheometrics-ARES constant strain rheometer. This ARES-rheometer is equipped with two torque transducers (2K FRTN1 and 2K FRTN1E) that can detect torques within the range 0.002−200 10^{-3}N m and normal forces within the range 0.02−20 N. An air oven with N_2 cooling allows a temperature range of −150 to +600 °C to be covered. The motor is a STD motor with a strain amplitude of 0.05−500 mrad and a rotation frequency varying between 10^{-5} and 500 rad s^{-1}.

During Fourier transform rheology, we have used an ADC-212 virtual oscilloscope from Virtual Instrument to record simultaneously the shear amplitude and the shear torque versus time. The data from the transducers are digitized with

Table 1. Chain Structure, Polydispersity, Zero-shear Viscosity η_0, Cole−Cole Relaxation Time λ_c, and Elastic Compliance $J = \lambda_c/\eta_0$ Determined at 150 °C and Pulsation ω_1 (= 0.07/λ_c) Used for FTR Experiments at Fixed Dimensionless Frequencies

	chain structure								
	linear		sparsely branched						densely branched[a]
	LM1	LM2	BM1	BM2	BM3	BM4	BM5	BM6	BR1
M_n (kg/mol)	30.4	18.5	15.1	16.9	17.2	19.3	18.1	15.4	-
M_w (kg/mol)	74	92	219	145	220	169	241	116	-
polydispersity	2.4	5	14.5	8.6	12.8	8.8	13.3	7.5	-
η_0 (Pa s)	4896	5840	71 090	108 630	138 920	194 850	138 305	49 360	35 063
λ_c (s)	0.022	0.092	2.32	9.46	4.04	13.11	4.07	5.93	4.25
J (Pa^{-1})	4.6×10^{-6}	1.6×10^{-5}	3.3×10^{-5}	8.6×10^{-5}	3.0×10^{-5}	6.6×10^{-5}	2.9×10^{-5}	1.2×10^{-4}	1.2×10^{-4}
$\omega_1 = 0.07/\lambda_c$ (rad s^{-1})	3.2×10^{0}	7.6×10^{-1}	3.0×10^{-2}	7.4×10^{-3}	1.7×10^{-2}	5.3×10^{-3}	1.7×10^{-2}	1.2×10^{-2}	1.6×10^{-2}

[a] Because of the difficulty dissolving BR1 in TCB, no SEC measurements have been carried out for this PE.

a 12-bit analogue-to-digital converter, operating at a sampling rate of 3 million samples per second. The connections between the ARES rheometer and the Virtual oscilloscope are realized with BNC-type cables. The Picolog software from Virtual Instrument permits collection of the data directly on the computer in the form of tables.

Experimental Procedures. To process all rheological tests on the ARES rheometer, samples were first carried out at 150 °C under a pressure of 20 MPa into 15-mm diameter disks with a thickness of 3 mm. We have checked the nondegradation of the samples to avoid chain extension or cross-linking during experiments. We have performed dynamical measurements of dynamical modulus at 150, 180, and 210 °C for all the samples on a large time scale. We have noticed that thermal degradation of the polymers at 150 °C could be excluded within the error margin simply because G' and G'' did not change over several hours at 150 °C with a frequency of 0.5 rad s^{-1} and a strain amplitude of 10%.

For all rheological experiments, the test temperature was 150 °C. For small deformation mechanical spectrometry, the geometry was parallel plates of 25 mm diameter with a gap of 0.5 mm, the frequencies were in the range 0.01−100 rad s^{-1} and with a strain amplitude of 10%. To reach the terminal flow, additional linear viscoelastic measurements have also been carried out at 210 °C. For Fourier transform rheology (FTR), the configuration of the test was cone-plate geometry with a diameter of 25 mm and an angle of 5°. To test the stability of the samples regarding thermal degradation and material loss due to the Weissenberg effect, small deformation mechanical spectrometry has been carried out in the range 1−100 rad s^{-1} before and after each FTR measurement. Zero-shear viscosity η_0 has been obtained by creep measurements at a constant stress of 100 Pa during 45 min to reach the plateau. For all rheological experiments, the reproducibility was checked by repeating the measurements at least two times (with changing the sample): the variability was less than 5%.

3. Experimental Results

3.1. Cole−Cole Relaxation Time λ_c and Zero-Shear Viscosity η_0. Table 1 shows the Cole−Cole relaxation time λ_c and the zero-shear viscosity η_0. The characteristic time λ_c corresponds to the inverse of the frequency ω_c for which the Cole−Cole diagram reaches a maximum. When the determination of λ_c was not directly possible on the Cole−Cole diagram, we used the Schmitt diagram (see Fleury et al.[40]). As reported by Vega et al.,[16] λ_c is much lower for linear than for branched polyethylenes. As the zero-shear viscosity and the Cole−Cole relaxation time rise from the whole chain structure (molecular weight and its distribution and branching), we have plotted in the log−log space η_0 and λ_c against M_w (see Figure 1a and b) to highlight the effect of branching from the effect of molecular weight. It clearly appears that η_0 and λ_c of BM2, BM6, and BM4 significantly deviate from that of the group of LM1, LM2, BM1, BM3, and BM5. Unfortunately, the measure of η_0 and λ_c against M_w does not show significant difference between the linear polymers LM1 and LM2 and the two highly polydisperse polyethylenes BM1, BM3, and BM5. Because, at constant molecular weight, branching density increases chain entanglements while it decreases the radius of gyration, a simple estimation of η_0 and λ_c is not sufficient to distinguish linear PE from sparsely branched PE. Thus, more relevant methods have to be considered.

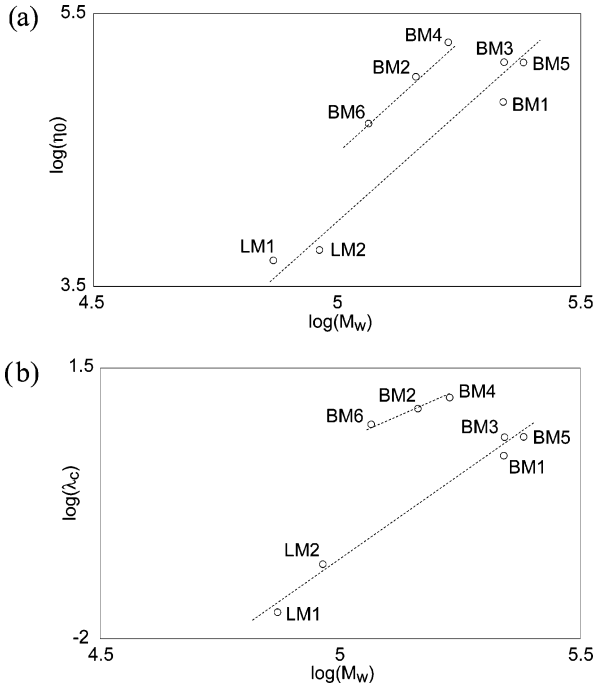

Figure 1. (a) Zero-shear viscosity η_0 and (b) Cole−Cole relaxation time λ_c as a function of molecular weight M_w for LM1, LM2, and BM1−BM6.

3.2. Mechanical Spectrometry in the Linear Domain, van Gurp−Palmen Plot. Figure 2 shows the van Gurp−Palmen curves (phase shift δ versus absolute value of the complex modulus $|G^*|$) of each polyethylene. To reach the terminal flow, additional measurements at 210 °C have been carried out. Unfortunately, except for linear polymers LM1 and LM2 and for branched polymer BR1, phase shift δ did not exceed 72°. As we can see, there are three distinct groups: the group of linear polymers (LM1 and LM2), the group of branched polymers (BM1−BM6), and the group of the lone-branched polyethylene BR1. The curves of LM1 and LM2 have a classical shape: From low to high $|G^*|$, the

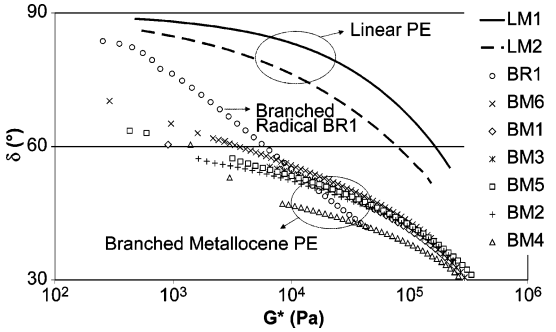

Figure 2. van Gurp−Palmen plots of linear and branched polyethylene at a reference of 150 °C.

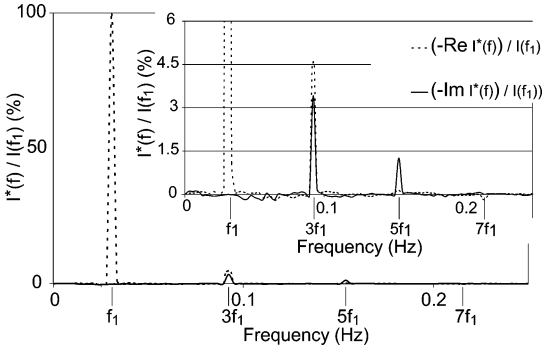

Figure 3. Normalized frequency spectrum of the torque of BM6 obtained at $\gamma_0 = 450\%$, $\omega_1 = 0.193$ rad s^{-1}, and $T = 150$ °C.

phase shift δ starts from a plateau at 90° then decreases. Because of the crystallization, the plateau modulus G_N^0 ($= G'(\omega|_{\delta \text{ at min}})$) is not reached for our samples. As Trinkle and Friedrich[22] have shown, the higher degree of polydispersity ($DP_{LM2} > DP_{LM1}$), the more the curves are stretched at low $|G^*|$. The second group, corresponding to the branched polyethylenes BM1−BM6, has lower δ, i.e., higher elasticity, than that of the previous group of linear PEs, which is in agreement with the results of Trinkle et al.[23] and Vega et al.[16] A vertical shift should be necessary to superimpose the data of LM1. This result seems to confirm the presence of long branching for BM1−BM6 (Mavridis and Shroff[42]). The curve of BM4 is the most stretched. This result means that BM4 should have the longest arms. Unfortunately, the van Gurp−Palmen plot is not able to differentiate the other branched PE between themselves. The latest PE, BR1, performed by radical synthesis, has a different behavior: δ starts from a plateau near 90° then decreases very rapidly. This result should be explained by the fact that the molecular structure of BR1 is distinguished from BM1−BM6 by a high number of short branches.

3.3. Fourier Transform Rheology. Principle and Methodology of FTR. Fourier transform rheology, as it is called by Wilhelm,[34−36] has been theoretically and experimentally well described (Giacomin and Dealy[43] and Wilhelm et al.[34−36]). First, mechanical spectrometry is carried out at high strain $\gamma(t) = \gamma_0 \sin(\omega_1 t)$, for which the validity of linear viscoelasticity fails. Indeed, although the torque response keeps its periodicity, it cannot be represented by a single harmonic function. Second, FTR consists of analyzing the frequency spectrum of the response in the Fourier space. The observed nonlinear effects are related to: (a) shear thinning, which explains the squeeze of the torque signal near its maxima and minima, and (b) viscoelasticity, which induces a dissymmetry compared to the vertical line crossing the maximum value of the torque (see also Fleury et al.[40]). However, it must be noticed that, because of polymer viscoelasticity, the periodicity is not instantaneously established. Thus, the recording of the signal has been done after a minimum time, ensuring a quasi steady-state flow that validates the Fourier analysis.

The frequency spectrum of the torque has been obtained both by discrete Fourier transformation (see Fleury et al.[40]) and by a least-squares method. When using discrete fast Fourier transformation (DFT), a Hanning windowing has been used to filter the signal of the torque. Figure 3 shows a complex frequency spectrum of the torque obtained by discrete fast Fourier transformation. The real and the imaginary parts of the complex intensity of the spectrum $I^*(f)$ are represented relative to the intensity I_1 ($= I(f_1)$) of the complex intensity I^*_1 ($= I^*(f_1) = I^*(\omega_1)$) of the fundamental frequency ω_1. Because of the relationship between the viscosity and the absolute value of the shear rate $\eta(|\dot\gamma|) = \eta(\dot\gamma) = \eta(-\dot\gamma)$, the spectrum shows only odd harmonics (Wilhelm et al.[34,36]). Consequently, the torque can be written according to the following expression:

$$T(t) = I_1 \, e^{i(\omega_1 t+\varphi_1)} + I_3 \, e^{i(3\omega_1 t+\varphi_3)} + I_5 \, e^{i(5\omega_1 t+\varphi_5)} + I_7 \, e^{i(7\omega_1 t+\varphi_7)} + \ldots \quad (1)$$

The least-squares method consisted in fitting the experimental torque signal with the following function:

$$T(t) = I_2 \cos(2\omega_1 t + \varphi_2) + \sum_{n=1}^{6} I_{2n-1} \cos[(2n-1)\omega_1 t + \varphi_{2n-1}] \quad (2)$$

where the additional term $I_2 \cos(\omega_2 t + \varphi_2)$ takes into account the noise. It appears that both the DFT and least-squares methods lead to the same values of I_3, I_5, φ_3, and φ_5.

Figure 3 shows that the relative intensities of odd harmonics decrease with respect to frequency. Thus, the relative complex intensity

$$I^*_3/I_1 \left(= \frac{I^*(3f_1)}{I_1} = \frac{I_3}{I_1} e^{3i\omega_1 t} \right)$$

gives an idea of nonlinear effects of the first order. The analysis will further consist in characterizing nonlinear effects by the study of the modulus of the relative intensities I_3/I_1 with respect to strain amplitude γ_0 and the study of the real and the imaginary parts of I^*_3/I_1. A first series of measurements has been carried out at constant pulsation $\omega_1 = 0.193$ rad s^{-1}. A second series of measurements has been carried out at fixed dimensionless frequency $\omega_1\lambda_c = 0.07$.

Analysis of the Intensity of the Relative Harmonic I_3/I_1. Figure 4 compares the relative third harmonic I_3/I_1 versus γ_0 of polyethylene obtained at constant frequency $\omega_1 = 0.193$ rad s^{-1} and those obtained at constant dimensionless frequency $\omega_1\lambda_c = 0.07$. As it was previously observed,[40] the experiments carried out at constant ω_1 show two distinct groups: the group of linear polymers LM1 and LM2 and the group of branched polymers. Indeed, nonlinear effects characterized by the level of the relative third harmonic I_3/I_1 are much higher for branched polymers than for

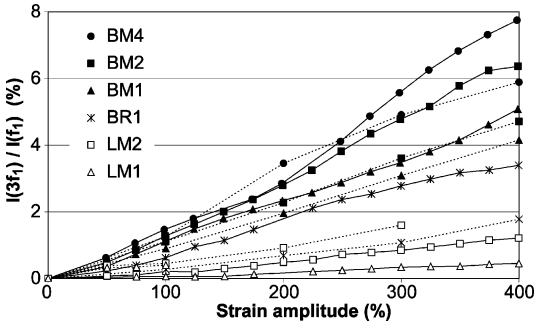

Figure 4. Relative intensity of the third harmonic I_3/I_1 as a function of strain amplitude γ_0 of linear and branched polyethylene at $T = 150$ °C for: $\omega_1 = 0.193$ rad s^{-1} (—) and $\omega_1\lambda_c = 0.07$ (- - -).

linear polymers. As molecular weights of each polymer are of the same order, the drastic increase of I_3/I_1 for polymers BM1−BM6 and BR1 can be explained by the effect of their LCB. However, as LM1 and LM2 have characteristic relaxation times λ_c much smaller than those of branched ones (see Table 1), the fixed frequency ($\omega_1 = 0.193$ rad s^{-1}) chosen for this series of experiments is located in the flow region for linear polymers, whereas it is located near the plateau zone for the branched ones. Thus, effects of entanglements on I_3/I_1 could be more pronounced for branched polymers than for linear ones. To avoid this, a series of experiments at fixed dimensionless frequency $\omega_1\lambda_c = 0.07$ have been carried out. Table 1 shows the corresponding frequencies ω_1 used for thise series of experiments. The relatively low value of $\omega_1\lambda_c$ allows testing of the polymers near the flow region where the branching points should exhibit higher nonlinear effects regarding entanglements. A lower value of $\omega_1\lambda_c$ would have led to too-long acquisition times for branched polymers. In addition, because of the high ω_1 for linear polymers ($\omega_1 = 3.2$ rad s^{-1} for LM1 and $\omega_1 = 0.76$ rad s^{-1} for LM2), the Weissenberg effect has been observed for strains higher than 100% for LM1 and 300% for LM2, which explains the lack of data for linear polymers. Nevertheless, at fixed dimensionless frequency $\omega_1\lambda_c$, the levels of I_3/I_1 observed for LM1−LM2 remain much lower than for those observed for BM1−BM6. Furthermore, the classification of the polymers (LM1−LM2 and BM1−BM6) obtained from the lowest up to highest I_3/I_1 is the same as that obtained for the experiments at fixed ω_1. Polymer BR1 shows particular behavior. Indeed, it is the only branched polymer for which the degree of nonlinearity (I_3/I_1) decreases drastically with the frequency.

Phase Shift and Niquist Diagrams of the Complex Relative Harmonic I^*_3/I_1. Nonlinear effects cannot be explained from the unique study of I_3/I_1. Consequently, the study of the whole complex relative intensity I^*_3/I_1 is necessary to go deeper in the understanding of the correlation between the FTR results and the macromolecular structure. To evaluate all the results compared to the same reference timeframe, a consistent method has been proposed by Neidhöfer et al.[44] If one writes the real part of the function $T(t)$, one obtains:

$$T(t) = I_1 \cos(\omega_1 t + \varphi_1) + I_3 \cos(3\omega_1 t + \varphi_3) + \ldots \quad (3)$$

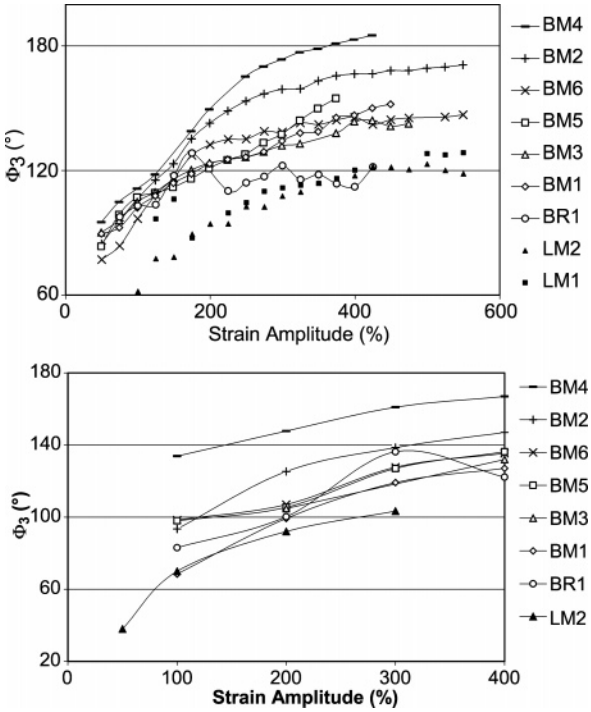

Figure 5. Phase shift Φ_3 of the third complex relative harmonic $I(3f_1)/I(f_1)$ of linear and branched polyethylene obtained at $T = 150$ °C and: (a) $\omega_1 = 0.193$ rad s^{-1}, (b) $\omega_1\lambda_c = 0.07$.

If one shifts the time scale thanks to the following substitution:

$$t = t' - \frac{\varphi_1}{\omega_1} \quad (4)$$

It gives the following expression of the torque:

$$T(t) = I_1 \cos(\omega_1 t') + I_3 \cos(3\omega_1 t' + \Phi_3) + \ldots \quad (5)$$

With:

$$\Phi_3 = \varphi_3 - 3\varphi_1 \quad (6)$$

Thus, Φ_3 corresponds to the phase shift between the third harmonic I^*_3 and the fundamental I^*_1, which is purely real in such a reference timeframe. Neidhöfer et al.[44] have shown that, thanks to this choice, the phase shift Φ_3 is a picture of the rheological behavior. For example, shear thinning behavior corresponds to $\Phi_3 = 180°$, while shear thickening corresponds to $\Phi_3 = 0°$ or $\Phi_3 = 360°$. Furthermore, for all the other cases, the torque shows a mirror asymmetry compared to the vertical line passing by the maximum: the maxima and the minima are shifted to the left side for $0 < \Phi_3 < 180°$, while the maxima and the minima are shifted to the right side for $\Phi_3 > 180°$.

Figure 5a shows the phase shift Φ_3 of the third harmonic as a function of the strain amplitude γ_0 obtained $\omega_1 = 0.193$ rad s^{-1}. For each polyethylene, Φ_3 increases faster for low γ_0 before reaching a plateau. At fixed ω_1, the linear polymers LM1 and LM2 reach a plateau near 120°, while the metallocene-catalyzed branched polymers BM1−BM6 reach a plateau at higher Φ_3. Furthermore, phase shift Φ_3 of BM4 is the highest, exceeding 180° for $\gamma_0 > 400\%$ and equal to 180° at $\gamma_0 = 365\%$, which means that the polymer has a pure

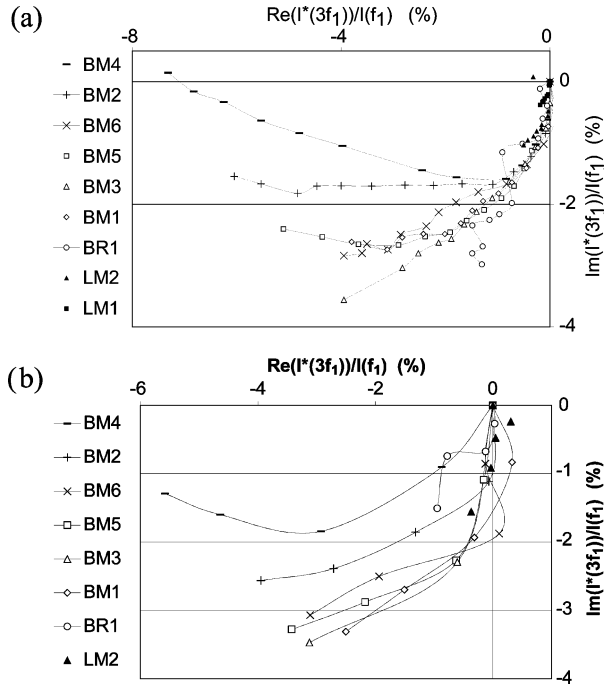

Figure 6. Niquist diagram of the third complex relative harmonic $I(3f_1)/I(f_1)$ of linear and branched polyethylene obtained at $T = 150$ °C and: (a) $\omega_1 = 0.193$ rad s^{-1} from $\gamma_0 = 0$ up to 375%, (b) $\omega_1\lambda_c = 0.07$ from $\gamma_0 = 0$ up to 400% except for LM2, where $\gamma_0 = 0$ up to 300%.

shear thinning behavior at this strain. Let us define the phase shift at low strain amplitude:

$$\Phi_3{}^0 = \Phi_3(\gamma_0 = 0) \tag{7}$$

We can notice that $\Phi_3°$ is much lower for linear polyethylenes LM1 and LM2 than for the others. Polymer BR1 has a typical behavior: at low strain amplitude, the evolution of Φ_3 against γ_0 is similar to metallocene-branched polyethylenes BM1−BM6, while at high strains, it reaches the same plateau as linear polyethylenes LM1−LM2. The results of Φ_3 versus γ_0, obtained at constant dimensionless frequency $\omega_1\lambda_c = 0.07$, are shown in Figure 5b. Although Φ_3 is a little bit lower than those measured at constant frequency, one observes the same classification: LM2 has the lowest Φ_3, whereas BM2 and even more BM4 have the highest phase shift Φ_3. Surprisingly, Φ_3 of BR1 shows values fluctuating with γ_0 as already observed for the experiments at fixed ω_1.

Figure 6 shows Niquist diagrams where the imaginary part of I^*_3/I_1 is plotted against the real part of I^*_3/I_1 obtained at: (a) $\omega_1 = 0.193$ rad s^{-1} and (b) $\omega_1\lambda_c = 0.07$. This Niquist diagram seems to be relevant to differentiate the different polymer behaviors. Indeed, the graphs of linear polymers are located near the origin of the diagram (because I_3/I_1 is low compared to that of branched polymers), while the graphs of branched polymers are more stretched. The graph of BM4 is the most stretched, and one observes that the imaginary part of I^*_3/I_1 starts to decrease for small strain amplitudes (i.e., near the origin of the Niquist diagram) before increasing for higher strains.

4. Constitutive Models

4.1. Wagner−Stephenson Integral Model. In this study, we used the following Wagner−Stephenson model (Wagner and Stephenson[45]), which derives from the single integral constitutive K-BKZ model:

$$\tau(t) = \int_{-\infty}^{t} m(t - t')H(t,t')C^{-1}_{(t,t')}\,\mathrm{d}t' \tag{8}$$

where $\tau(t)$ is the viscoelastic extra-stress tensor at time t, $m(t - t')$ is the memory function, $C^{-1}_{(t,t')}$ is the Finger strain tensor and $H(t,t')$ is the damping function.

The memory function is defined by a generalized Maxwell model:

$$m(t - t') = \sum_{i=1}^{N} m_i(t - t') = \sum_{i=1}^{N} \frac{G_i}{\lambda_i}\,\mathrm{e}^{-(t-t')/\lambda_i} \tag{9}$$

where G_i and λ_i are the relaxation spectrum corresponding to the linear viscoelastic behavior (i.e., corresponding to the polymer behavior at small strains).

The functional $H(t,t')$ takes into account the strain-dependent network disentanglements. Moreover, $H(t,t')$ proposed by Wagner and Stephenson[45] takes into account the irreversibility of network disentanglements when the strain decreases:

$$H(t,t') = \min_{t''\in[t',t]} [h(\gamma(t'',t'))] \tag{10}$$

where $h(\gamma)$ is the damping function, which is given by the following equation for shear flow:

$$h(\gamma) = \frac{1}{1 + a\gamma^b} \tag{11}$$

The damping function has been chosen in the form of eq 11 because its consistency with the Doi−Edward theory for which $b = 2$ (see Larson[46] and Khan and Tanner[47]).

For oscillatory shear flow, $\gamma(t,t')$ is defined as:

$$\gamma(t,t') = \gamma_0(\sin(\omega t) - \sin(\omega t')) \tag{12}$$

Equation 8 has been used to estimate the stress during simple oscillatory shear flows. It must be mentioned that the integration of eq 8 has to be performed with special care. Indeed, for low relaxation time λ_i, the time step has to be adapted when integrating near $t' = t$ to take into account the huge increase of the memory function. Then, Fourier transformations of $\tau(t)$ have been used to calculate I_3/I_1, I^*_3/I_1, and Φ_3 against γ_0. For a one-mode Maxwell fluid ($G = G_1 = 10^5$ Pa and $\lambda = \lambda_1 = 5$ s), we have tested the influence of parameters a and b from the damping function of the Wagner−Stephenson model.

Figure 7 shows the effects of a and b from the damping function on I_3/I_1 versus γ_0. As expected, an increase of parameter a or b involves an increase of nonlinear effects characterized by I_3/I_1. We can notice that parameter a affects I_3/I_1 (represented by the dashed lines) because of the lower values of γ_0, while parameter b increases I_3/I_1 from only $\gamma_0 = 50\%$. Figure 8 shows the influence of a and b on the phase shift Φ_3 as previously defined. Whatever the value of a and b, Φ_3 increases with γ_0. Furthermore, the dashed lines of the graph show that if the power b of the damping function keeps constant, the value of $\Phi_3{}^0$ also keeps constant. Thus, parameter a allows control of the increase of the phase shift Φ_3 from an initial value $\Phi_3{}^0$ obtained from parameter b. Moreover, Figure 9 shows that parameters

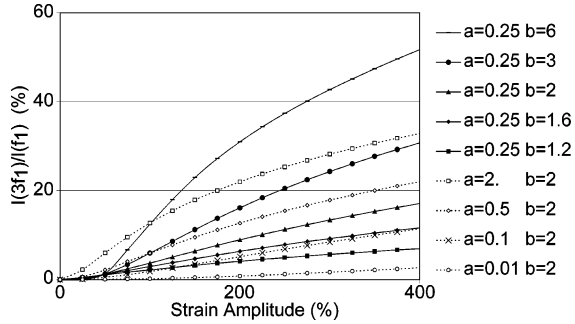

Figure 7. Effect of parameters (a) and (b) from the Wagner law on the third complex relative harmonic $I(3f_1)/I(f_1)$ for a one-mode Maxwell polymer ($G = 10^5$ Pa, $\lambda = 5$ s) at $\omega_1 = 0.193$ rad s^{-1}.

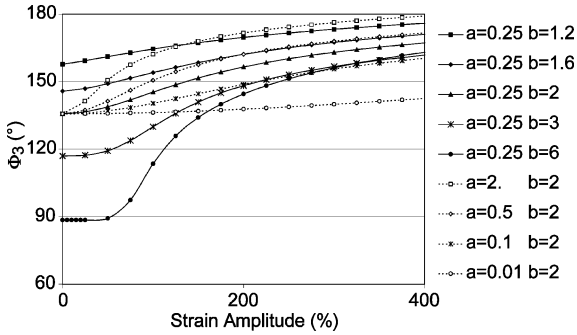

Figure 8. Effect of parameters (a) and (b) from the Wagner law on the phase shift Φ_3 of the third complex relative harmonic $I(3f_1)/I(f_1)$ for a one-mode Maxwell polymer ($G = 10^5$ Pa, $\lambda = 5$ s) at $\omega_1 = 0.193$ rad s^{-1}.

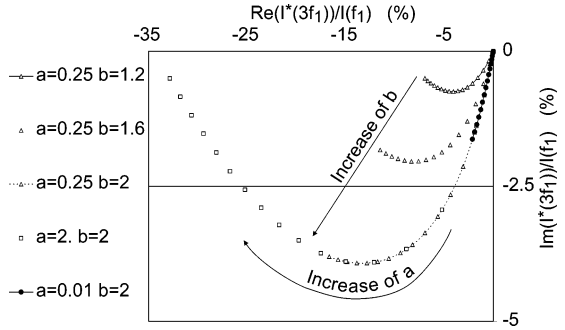

Figure 9. Effect of parameters (a) and (b) from the Wagner law on the Niquist diagram of the third complex relative harmonic $I(3f_1)/I(f_1)$ for a one-mode Maxwell polymer ($G = 10^5$ Pa, $\lambda = 5$ s) at $\omega_1 = 0.193$ rad s^{-1} from $\gamma_0 = 0$ up to 400%.

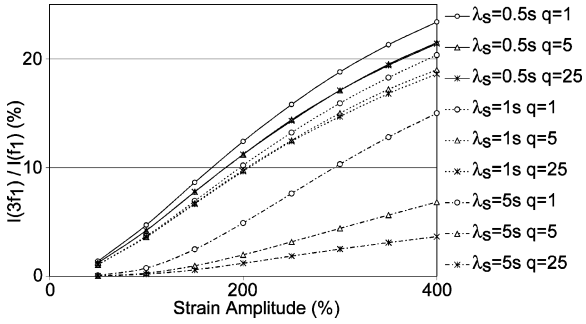

Figure 10. Effect of parameters λ_s and q from the pompom model on the third complex relative harmonic $I(3f_1)/I(f_1)$ for a one-mode Maxwell polymer ($G = 10^5$ Pa, $\lambda = 5$ s) at $\omega_1 = 0.193$ rad s^{-1}.

a and b allow precise control of the curve of the Niquist diagram of I^*_3/I_1. Thus, for a given range of γ_0, each value of b leads to a specific curve shape, whereas parameter a controls the position along this curve.

4.2. Differential Multimode Pompom Model. A differential multimode pompom model has been used for the simulation of FTR to provide more insight into macromolecular structural effects. In our work, we have used the time evolution of the extra-stress tensor τ, which is given by the following set of equations (Clemeur et al.[39] and Lee et al.[48]):

$$\tau = \sum_{i=1}^{N} G_i(3\Lambda_i^2 S_i - I) \tag{13}$$

$$\frac{1}{\lambda*_i}\left(S_i - \frac{I}{3}\right) + \Lambda_i^2 \overset{\nabla}{S}_i + 2\Lambda_i^2 (L{:}S_i)S_i = 0 \tag{14}$$

$$\lambda_{si}\frac{D\Lambda_i}{Dt} - \lambda_{si}(L{:}S_i)\Lambda_i + (\Lambda_i - 1)\, e^{2/q_i(\Lambda_i - 1)} = 0 \quad \text{for } \Lambda_i < q_i \tag{15a}$$

$$\frac{D\Lambda_i}{Dt} = 0 \quad \text{for } \Lambda_i = q_i \tag{15b}$$

with:

$$\frac{1}{\lambda_i^*} = \frac{1}{\lambda_i} \quad \text{for } 1 \le \Lambda_i \le q_i \tag{16a}$$

$$\frac{1}{\lambda_i^*} = \frac{1}{\lambda_i} + \frac{1}{\Lambda_i}\frac{D\Lambda_i}{Dt} - (L{:}S_i) \quad \text{for } \Lambda_i < 1 \tag{16b}$$

where G_i is the plateau modulus and λ_i the relaxation time of the ith mode obtained from the linear viscoelastic behavior (Inkson et al.[12]), N is the number of Maxwell modes, L is the transposition of the velocity gradient, S_i describes the average backbone tube orientation, Λ_i is the backbone tube stretch, λ_{si} is the relaxation time of the stretch, and q_i is the number of pompom arms. The introduction of time λ_i^* in eq 14 allows taking into account the reverse flow (Lee et al.[48]). Indeed, eq 16b permits the tube to retract faster than the chain, which may occur when sign of the strain rapidly changes. $\overset{\nabla}{S}_i$ is the upper convected time derivative of S_i, defined as:

$$\overset{\nabla}{S}_i = \frac{\partial S_i}{\partial t} - LS_i - S_iL^T \tag{17}$$

The set of eqs 13−17 have been solved for simple oscillatory shear flows. Then, the resulting shear component of the stress tensor has been studied thanks to Fourier analysis. For a one-mode Maxwell fluid ($G = G_1 = 10^5$ Pa and $\lambda = \lambda_1 = 5$ s), we have tested the influence of the pompom parameters (i.e., the number of arms $q = q_1$ and the relaxation time of the stretch $\lambda_s = \lambda_{s1}$) on I_3/I_1 and I^*_3/I_1 versus γ_0.

Figure 10 shows the evolution of the relative third harmonic intensity I_3/I_1 against γ_0 for different values of λ_s and q. It appears that an increase of the number of pompom arms q at constant stretch relaxation time λ_s leads to the decrease of I_3/I_1. The same tendency is observable when λ_s decreases for a given value of q. Figure 11 shows the Niquist diagrams of I^*_3/I_1 for the different values of q and λ_s. As for the previous result, the increase of q (or the decrease of λ_s) decreases nonlinear effects characterized by the intensity of the real and the imaginary parts of I^*_3/I_1. We have to

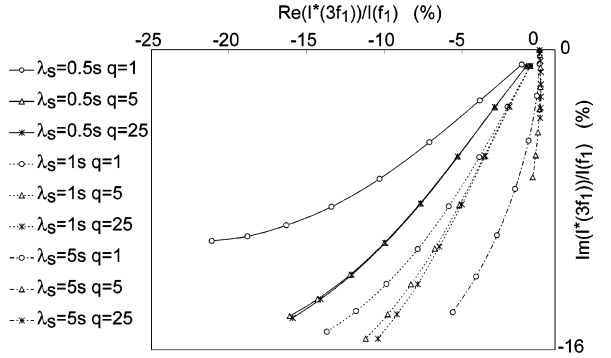

Figure 11. Effect of parameters λ_s and q from the pompom model on the Niquist diagram of the third complex relative harmonic $I(3f_1)/I(f_1)$ for a one-mode Maxwell polymer ($G = 10^5$ Pa, $\lambda = 5$ s) at $\omega_1 = 0.193$ rad s^{-1} from $\gamma_0 = 0$ up to 400%.

Table 2. Parameters for Maxwell, Wagner, and Pompom Models for LM1 at 150°C

Maxwell		Wagner		pompom		
G_i (Pa)	λ_i (s)	a_i	b_i	q_i	λ_{si} (s)	λ_i/λ_{si}
6.2×10^5	8×10^{-4}	1	2	1	8×10^{-5}	10
2.5×10^5	6.4×10^{-3}	1	2	1	8×10^{-4}	8
3.3×10^4	2.6×10^{-2}	1	2	1	6.4×10^{-3}	4
1.7×10^4	5.1×10^{-2}	0.4	2.5	1	2.6×10^{-2}	2
3.1×10^3	2×10^{-1}	0.12	4.5	1	5.1×10^{-2}	4
1.7×10^2	1×10^0	0.03	3.7	1	2×10^{-1}	5
9×10^1	2×10^0	0.03	3.2	1	1×10^0	2
2×10^0	6×10^0	0.02	5	1	2×10^0	3

Table 3. Parameters for Maxwell, Wagner, and pompom Models for LM2 at 150°C

Maxwell		Wagner		pompom		
G_i (Pa)	λ_i (s)	a_i	b_i	q_i	λ_{si} (s)	λ_i/λ_{si}
3×10^5	4×10^{-4}	1	2	1	4×10^{-4}	1
4.5×10^5	8×10^{-4}	1	2	1	8×10^{-4}	1
8.6×10^4	6.4×10^{-3}	1	2	1	6.4×10^{-3}	1
5.4×10^4	1.3×10^{-2}	1	2	1	1.3×10^{-2}	1
4.8×10^3	2.5×10^{-2}	1	2	1	2.5×10^{-2}	1
2.3×10^4	5×10^{-2}	0.5	2.5	1	5×10^{-2}	1
5.4×10^3	2×10^{-1}	0.18	3	1	2×10^{-1}	1
9.1×10^2	8×10^{-1}	0.045	3	1	5×10^{-1}	1.6
1.7×10^2	3.3×10^0	0.045	3	2	1.6×10^0	2
7.1×10^0	5.2×10^1	0.075	4	2	2.6×10^1	2

mention that calculations have been done for a given set of parameters G, λ which depends itself on the molecular weight and the molecular structure.

5. Comparison between Experiments and Models, Discussion

Both the Wagner−Stephenson integral model and the differential multimode pompom model have been used to investigate the behavior of each studied polyethylene during FTR experiments at 150 °C regarding the complex relative intensity I^*_3/I_1. All the results are summarized in Tables 2−10. The experimental linear viscoelastic spectra have been modeled thanks to the generalized Maxwell model. For a given set of relaxation times λ_i, the fitted values of G_i have been obtained from a least-squares method. Then, nonlinear parameters of each model have been obtained by fitting the numerical Niquist diagrams of I_3^*/I_1 with the experimental ones obtained at fixed frequency $\omega_1 = 0.193$ rad s^{-1}. Unfortunately, linear viscoelastic experiments carried out for metallocene-branched polymers BM1−BM6 did not allow reaching a loss angle δ greater than 72°. Thus, the discrete relaxation spectra are not very well defined for the lowest frequencies where branches play an important role regarding rheological properties. For the irreversible Wagner model, it has appeared that a unique set of parameters (a, b) of the damping function (11) does not allow fitting of the experimental results from low up to large shear amplitudes γ_0. In fact, the set of eqs 8−12 is only able to model the evolution of the intensity I_3/I_1 versus γ_0 but not the Niquist diagram. To overcome this problem, we propose applying a damping function for each Maxwell mode. Thus, the following modified Wagner model is proposed:

Table 4. Parameters for Maxwell, Wagner, and Pompom Models for BM1 at 150°C

Maxwell		Wagner		pompom		
G_i (Pa)	λ_i (s)	a_i	b_i	q_i	λ_{si} (s)	λ_i/λ_{si}
7.2×10^4	1×10^{-4}	0.1	2	1	3.4×10^{-5}	2.9
4.6×10^5	5.6×10^{-4}	0.1	2	1	1.9×10^{-4}	2.9
1.6×10^5	3.2×10^{-3}	0.1	2	1	1.1×10^{-3}	2.9
1.3×10^5	1.8×10^{-2}	0.1	2	1	6×10^{-3}	3
5.9×10^4	1×10^{-1}	0.1	5	1	3.4×10^{-2}	2.9
3.5×10^4	5.6×10^{-1}	0.1	6	1	1.9×10^{-1}	2.9
2.6×10^3	3.2×10^0	0.6	2.8	1	3.2×10^0	1
6.8×10^3	6.6×10^0	0.2	1.7	1	6.6×10^0	1
2×10^3	3.3×10^1	0.25	1.5	4	16×10^0	2.1

$$\tau(t) = \int_{-\infty}^{t} \sum_{i=1}^{N} m_i(t - t')H_i(t,t')C^{-1}_{(t,t')}\,\mathrm{d}t' \tag{18}$$

$$H_i(t,t') = \min_{t'' \in [t',t]} [h_i(\gamma(t'',t'))] \tag{19}$$

where $h_i(\gamma)$ is a damping function associated to the ith Maxwell mode:

$$h_i(\gamma) = \frac{1}{1 + a_i\gamma^{b_i}} \tag{20}$$

Thanks to this, the modified Wagner model was able to characterize the behavior of each polyethylene in large-amplitude oscillatory shear from $\gamma_0 = 0$ up to 400% (see Figures 12 and 13). However, we must notice that the introduction of a damping function associated at each Maxwell mode does not allow verification of the time-strain separability that is generally observed for step−strain experiments (cf. Larson[46]).

Figure 12 shows that the differential pompom model is able to fit the curves of I_3/I_1 versus γ_0. Figure 13a and b compare the experimental data and the pompom model, respectively, for LM1, LM2, and for BR1, BM4, BM6. Surprisingly, Figure 13b shows that the pompom model fails to predict the Niquist diagram of I_3^*/I_1 for the branched polyethylene BM4. We encountered the

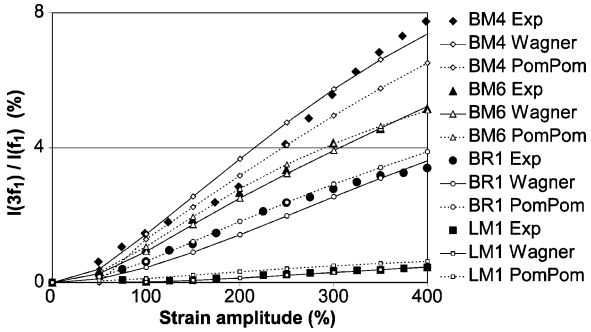

Figure 12. Comparison of experimental results and simulation of the relative intensity of the third harmonic I_3/I_1 as a function of strain amplitude γ_0 at $\omega_1 = 0.193$ rad s^{-1} and $T =$ 150 °C.

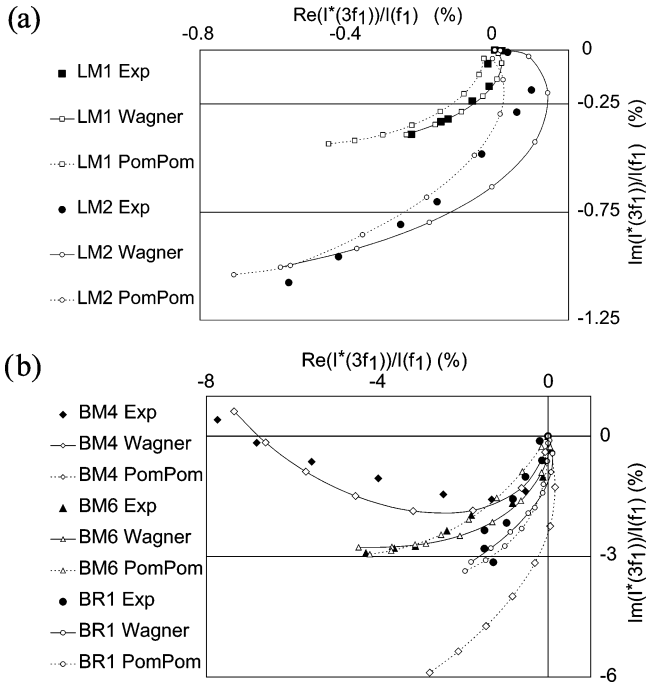

Figure 13. Comparison of experimental results and simulation of Niquist diagram of the third complex relative harmonic $I(3f_1)/I(f_1)$ obtained at $\omega_1 = 0.193$ rad s^{-1}, $T = 150$ °C from $\gamma_0 = 0$ up to 400% (a) for LM1 and LM2, (b) for BR1, BM6, and BM4.

Table 5. Parameters for Maxwell, Wagner, and Pompom Models for BM2 at 150°C

Maxwell		Wagner		pompom		
G_i (Pa)	λ_i (s)	a_i	b_i	q_i	λ_{si} (s)	λ_i/λ_{si}
2.5×10^5	1×10^{-4}	0.1	2	1	1×10^{-5}	10
2.6×10^5	5.6×10^{-4}	0.1	2	1	1×10^{-4}	5.6
2.1×10^5	3.2×10^{-3}	0.1	2	1	5.6×10^{-4}	5.7
1.1×10^5	1.8×10^{-2}	0.1	2	1	3.2×10^{-3}	5.6
5.4×10^4	1×10^{-1}	0.1	2	1	1.8×10^{-2}	5.6
2.1×10^4	5.6×10^{-1}	0.65	2.75	1	1×10^{-1}	5.6
8.8×10^3	3.2×10^0	0.15	2.55	1	5.6×10^{-1}	5.7
3.5×10^3	1.8×10^1	0.08	1.65	2	3.2×10^0	5.6

Table 6. Parameters for Maxwell, Wagner, and Pompom Models for BM3 at 150°C

Maxwell		Wagner		pompom		
G_i (Pa)	λ_i (s)	a_i	b_i	q_i	λ_{si} (s)	λ_i/λ_{si}
1×10^5	1×10^{-4}	0.1	2	1	1.9×10^{-5}	5.6
3.5×10^5	5.6×10^{-4}	0.1	2	1	1.5×10^{-4}	3.8
2×10^5	3.2×10^{-3}	0.1	2	1	8.2×10^{-4}	3.8
1.4×10^5	1.8×10^{-2}	0.1	2	1	4.7×10^{-3}	3.8
7.6×10^4	1×10^{-1}	0.1	2	1	2.6×10^{-2}	3.8
3×10^4	5.6×10^{-1}	0.1	2	2	1.5×10^{-1}	3.8
1.4×10^4	3.2×10^0	0.09	2.65	5	8.2×10^{-1}	3.8
3.5×10^3	1.8×10^1	0.065	1.65	10	4.7×10^0	3.8

same difficulties for BM2 and BM5. Consequently, we have to notice here that the parameters appearing in tables 5, 7, and 8 correspond to the best fit obtained only for I_3/I_1. On the other hand, it has been observed that the influence of nonlinear parameters of the modified Wagner and the pompom models associated with relaxation times shorter than 0.5 s is not significant.

Furthermore, experiments carried out at constant dimensionless frequency $\omega_1\lambda_c = 0.07$ have been modeled thanks to the parameters previously obtained by fitting experiments at constant frequency $\omega_1 = 0.193$ rad s^{-1}. Figures 14 and 15 compare experiments and models for

Table 7. Parameters for Maxwell, Wagner, and Pompom Models for BM4 at 150°C

Maxwell		Wagner		pompom		
G_i (Pa)	λ_i (s)	a_i	b_i	q_i	λ_{si} (s)	λ_i/λ_{si}
5.7×10^5	4×10^{-4}	0.08	2.6	1	4×10^{-5}	10
1.7×10^5	6.4×10^{-3}	0.08	2.6	1	4×10^{-4}	16
7.9×10^4	2.6×10^{-2}	0.08	2.6	1	6.4×10^{-3}	4
5.1×10^4	1×10^{-1}	0.08	2.6	1	2.6×10^{-2}	3.8
2.7×10^4	4×10^{-1}	0.55	2.65	1	1×10^{-1}	4
1.3×10^4	1.6×10^0	0.18	3.2	2	4×10^{-1}	4
1×10^4	6.5×10^0	0.125	2.4	2	1.6×10^0	4
3.5×10^3	2.6×10^1	0.05	1.025	2	6.5×10^0	4

Table 8. Parameters for Maxwell, Wagner, and Pompom Models for BM5 at 150°C

Maxwell		Wagner		pompom		
G_i (Pa)	λ_i (s)	a_i	b_i	q_i	λ_{si} (s)	λ_i/λ_{si}
2.6×10^5	1×10^{-4}	0.1	2	1	3.7×10^{-5}	2.7
2.3×10^4	5.6×10^{-4}	0.1	2	1	2.4×10^{-4}	2.3
3.2×10^5	3.2×10^{-3}	0.1	2	1	1.3×10^{-3}	2.5
1.7×10^5	1.8×10^{-2}	0.1	2	1	7.6×10^{-3}	2.4
9.4×10^4	1×10^{-1}	0.1	2	1	4.3×10^{-2}	2.3
3.7×10^4	5.6×10^{-1}	0.25	3.2	5	2.4×10^{-1}	2.3
2.2×10^4	3.2×10^0	0.15	1.85	10	1.3×10^0	2.5
1.9×10^3	1.8×10^1	0.01	1.2	10	7.6×10^0	2.4

the I_3/I_1 versus γ_0 plots and the Niquist diagrams, respectively. Good agreements are observed for LM1, LM2, and BM1. Good correlation has also been observed for BR1. For all other polymers, underestimations of I_3/I_1 (see for example the case of BM6 in Figure 14b) have been observed with modified Wagner and pompom models. This is still an open question for further investigations. Indeed, this discrepancy could be first allotted to the lack of viscoelastic data near the terminal flow but, as we can see in Table 9, BM6 was the branched polymer for which a linear viscoelastic spectrum has been obtained in a wide range of relaxation times. Moreover, all the calculations we performed thanks to the differential pompom model have shown

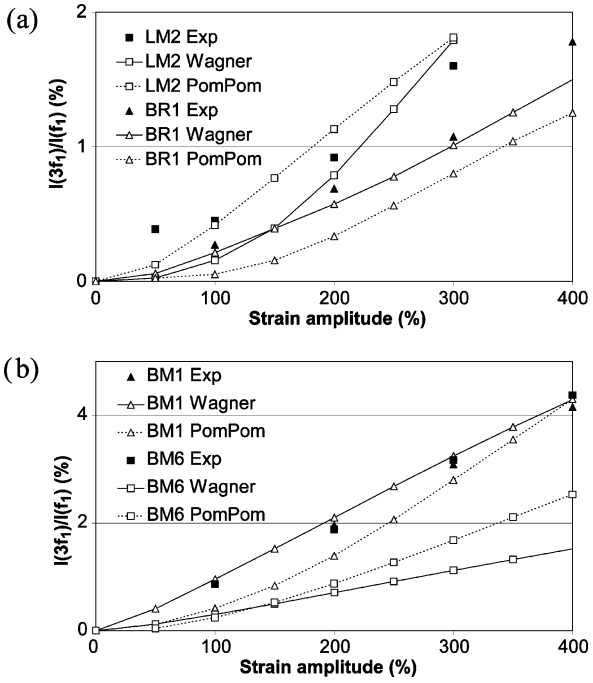

Figure 14. Comparison of experimental results and simulation of the relative intensity of the third harmonic I_3/I_1 as a function of strain amplitude γ_0 at $\omega_1\lambda_c = 0.07$ and $T = 150$ °C (a) for LM2 and BR1, (b) for BM1 and BM6.

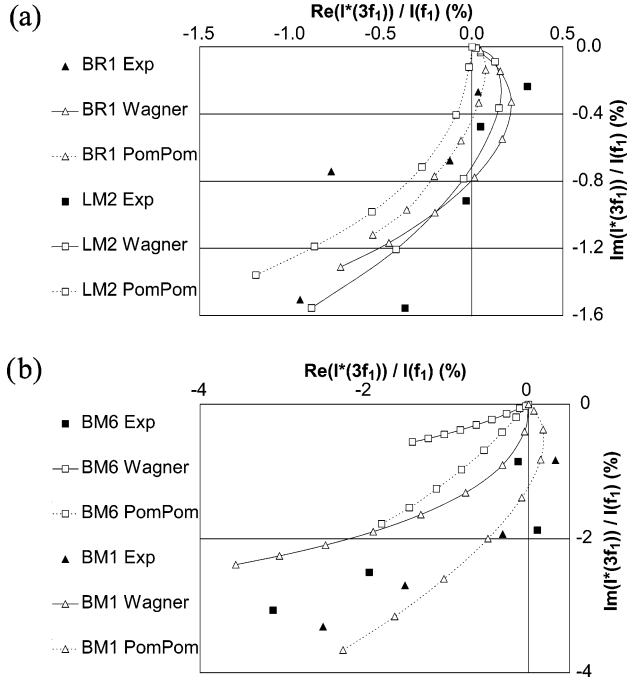

Figure 15. Comparison of experimental results and simulation of Niquist diagram of the third complex relative harmonic $I(3f_1)/I(f_1)$ obtained at $\omega_1\lambda_c = 0.07$, $T = 150$ °C from $\gamma_0 = 0$ up to 400% (a) for LM2 ($\gamma_0 = 0$ up to 300% in this case) and BR1, (b) for BM1 and BM6.

Table 9. Parameters for Maxwell, Wagner, and Pompom Models for BM6 at 150°C

Maxwell		Wagner		pompom		
G_i (Pa)	λ_i (s)	a_i	b_i	q_i	λ_{si} (s)	λ_i/λ_{si}
3.3×10^5	1×10^{-4}	0.1	2	1	1.7×10^{-5}	5.8
3.1×10^5	5.6×10^{-4}	0.1	2	1	1.4×10^{-4}	4.1
1.5×10^5	3.2×10^{-3}	0.1	2	1	7.7×10^{-4}	4.1
8.2×10^4	1.8×10^{-2}	0.1	2	1	4.4×10^{-3}	4.1
3.5×10^4	1×10^{-1}	0.1	2	1	2.5×10^{-2}	4.1
1.2×10^4	5.6×10^{-1}	0.1	5	1	1.4×10^{-1}	4.1
4.6×10^3	3.2×10^0	0.12	2.35	1	5.6×10^{-1}	5.7
1.3×10^3	1.8×10^1	0.12	1.6	2	4.5×10^0	4
1.6×10^2	2.0×10^2	0.12	1.6	3	2.0×10^1	10
2.0×10^2	5.0×10^2	0.12	1.6	4	2.0×10^2	2.5

Table 10. Parameters for Maxwell, Wagner, and Pompom Models for BR1 at 150°C

Maxwell		Wagner		pompom		
G_i (Pa)	λ_i (s)	a_i	b_i	q_i	λ_{si} (s)	λ_i/λ_{si}
5.9×10^5	1×10^{-4}	0.055	2.2	1	4.6×10^{-5}	2
2.9×10^5	3.2×10^{-3}	0.055	2.2	1	1.3×10^{-3}	2
2.5×10^4	1×10^{-1}	0.055	2.2	1	4.1×10^{-2}	2
9×10^3	5.6×10^{-1}	0.055	2.2	1	2.8×10^{-1}	2
3.1×10^3	3.2×10^0	0.055	2.2	100	1.6×10^0	2
3.7×10^2	1.8×10^1	0.055	2.2	100	9×10^0	2
9.8×10^1	1×10^2	0.055	2.2	100	5×10^1	2

that reverse flow characterized by a backbone tube stretch $\Lambda_i < 1$ occurs only at very high frequencies much higher than those experimentally tested.

Case of Linear Polyethylenes LM1 and LM2. The van Gurp−Palmen plot and FTR distinguish clearly the group of linear polyethylenes (LM1 and LM2) from the group of branched polyethylenes (BM1−BM6 and BR1). This result has been confirmed by several authors and can be explained by the fact that, as polyethylene is characterized far from the plateau zone, the effect of branched points are predominant in the effects of chain entanglements. Furthermore, each method highlights a difference between LM1 and LM2, which have a higher degree of polydispersity: (a) van Gurp−Palmen plots show a curve more stretched for LM2 than for LM1; (b) although the measured torque of LM1 and LM2 are identical, FTR shows higher level of nonlinear effects (characterized by I_3/I_1) for LM2. The fitting with the modified Wagner model shows high values of b_i and low values of a_i for long Maxwell relaxation times. Because of the supposed linear structure of LM1 and LM2, the first logical choice for the pompom parameters was $q_i = 1$ and $\lambda_{si} = \lambda_{i-1}$. This choice leads to good agreement with experimental results (see Figure 13a) for LM1. Surprisingly, the predicted results were not good for LM2. A value of $q = 2$ has to be taken to fit the experimental data. This choice should reflect that chains responsible for the mode corresponding to $q = 2$ are undergoing stretching within their tubes. This happens either because of long-chain branching or if the molecular weight is high enough. However, the fact that LM2 has been synthesized by the Ziegler−Natta technique leads to polyethylene without long branches but with possible presence of few short branches (Hamielec and Soares[41]). Thus, these short branches seem to play an important role on large-amplitude oscillatory shear experiments.

Case of Branched Polyethylenes BM1−BM6. This group of polymers has shown typical behavior compared to that of linear LM1 and LM2. Both van Gurp−Palmen plots and FTR experiments have clearly distinguished BM4, whose behavior shows the most pronounced differences with respect to that of linear polymers. Nevertheless, van Gurp−Palmen plots do not significantly distinguish the other branched PEs from one another. Thus, as it has been previously shown in Figure 9, an increase of b_N (corresponding to the longest relaxation time) should dilate the Niquist diagram. Thus, it appears that parameter b_N is lower for polymers whose behavior is the most different from that of linear polymer LM1. As for example, $b_{N-BM4} = 1.025$, while $b_{N-LM1} = 5$. On the other hand, it is interesting to notice the relative classification of BM2 and BM5. Indeed, SEC shows lower molar masses (M_n and M_w) and lower polydispersity for BM2 (see Table 1) than for BM5. These results are confirmed by a lower zero-shear viscosity and a lower level of the torque for BM2 measured during FTR experiments. Nevertheless, FTR experiments show that BM2, compared to BM5, has the diagram of I_3/I_1 versus γ_0 and the Niquist plot of I_3^*/I_1 the most distant from the group of linear polymers LM1−LM2. This result seems to indicate that the branches of BM2 play a more important role during large-amplitude oscillatory shear than those of BM5. All the experimental results (SEC and rheology) indicate that BM4 could have a molecular architecture similar as BM2. However, we must insist that, although the pompom model was able to fit I_3/I_1 versus γ_0, it was not possible to fit the Niquist diagram of I_3^*/I_1. Thus, it is not possible to discuss the values of the pompom model, in particular, for the branched polymers BM2, BM5, and also BM4, which have shown the most pronounced nonlinear behavior regarding to the level of I_3/I_1. Let us consider the results of BM1 and BM6 (respectively Tables 4 and 9), which have the same molecular weight M_n. FTR experiments show similar results regarding the Niquist diagram of I_3^*/I_1 (see Figure 6a and b). However, nonlinear parameters a_i and b_i of the modified Wagner

model and λ_{si} and q_i of the pompom model show some differences between BM1 and BM6: first, for the modified Wagner model, parameter a_7 (corresponding to $\lambda_7 = 3.2$ s) is much higher for BM1 than for BM6; second, for the pompom model, the time scale separation λ_i/λ_{si} is lower for BM1 than for BM6. As McLeish and Larson[10] have shown, the ratio λ_i/λ_{si} is proportional to the product of the normalized backbone molecular weight s_b and the fraction of the total molecular weight contained within the backbone Φ_b:

$$\frac{\lambda_i}{\lambda_{si}} \propto s_b \Phi_b \tag{21}$$

In other words, λ_i/λ_{si} is an indication of the distance between the branching points. Doerpinghaus and Baird[30] have observed that the effects of the separation in the relaxation time scales dominate the effects of the number of arms. As

$$\left.\frac{\lambda_i}{\lambda_{si}}\right|_{BM1} < \left.\frac{\lambda_i}{\lambda_{si}}\right|_{BM6}$$

the distance between branching points of BM1 should be lower than for BM6. Furthermore, if one introduces an elastic compliance as the ratio $J = \lambda_c/\eta_0$ (which is distinct to the recoverable elastic compliance $J_e^0 = \lambda_w/\eta_0$), one observes that J is higher for BM6 than for BM1 (see Table 1). This result is consistent with the observation following from the pompom model. As a consequence, we can expect that BM1 has more and shorter branches than BM6.

Case of Densely Branched Polyethylene BR1. This polyethylene, performed by radical synthesis, reveals a typical behavior. The van Gurp−Palmen plots (Figure 2) have shown a particular curve located between those of linear polyethylenes (LM1, LM2) and those of metallocene-branched polyethylenes (BM1−BM6). As it has been shown in figures 4, 5, and 6 at constant frequency $\omega_1 = 0.193$ rad s^{-1}, FTR experimental curves of BR1 are also located between those of linear polymers and those of branched polymers. The high elastic compliance J of BR1 (see Table 1), seems to indicate the presence of long branches. On the other hand, to fit the Niquist diagram of I^*_3/I_1 obtained from the pompom model with experiment, we had to consider a very high number of arms (q_5 to $q_7 = 100$) and low time scale separation ($\lambda_i/\lambda_{si} = 2$). Furthermore, we remind that near the terminal flow at $\omega_1\lambda_c = 0.07$, the level of I_3/I_1 is lower for BR1 than for LM2, meaning that the branches of BR1 play a minor contribution in this regime. All these results confirm the presence of a high number of short and long branches, which is typical for radical synthesis of polyethylene. Furthermore, it must be noticed that polymer BR1 was the only one for which a single set of Wagner parameters ($a = a_i = 0.055$ and $b = b_i = 2.2$ for $i = 1$ to N, in that case, the modified Wagner model is equivalent to the Wagner model with one separable damping function) allows fitting to the Niquist diagram of I^*_3/I_1.

6. Conclusions

Fourier transform rheology (FTR) consists of analyzing the frequency spectrum of the torque signal $I^*(f)$ obtained during large-amplitude oscillatory shear. The efficiency of FTR has been demonstrated for the study of branched polymers. FTR is sensitive to the architecture of polymers regarding molecular weight and its distribution, number of branches, and their length. It seems to be an experimental method that can substitute extensional measurements that are rather difficult to carry out. Furthermore, we have shown that the study of the frequency spectrum of the signal in the whole complex space allows getting more insight than only the study of the frequency spectrum's intensity. Associated with models, FTR is able to go deeper in the description of molecular structure. A modified Wagner integral model has been proposed. It consists of introducing a damping function for each Maxwell relaxation time. On the other hand, a differential multimode pompom model has also been used to model FTR experiments. Regarding the relative third complex harmonic I^*_3/I_1, the two models have been compared to experimental results obtained for nine different polyethylenes. The modified Wagner model was able to fit all experimental data carried out at constant frequency. It has been shown that parameter b_N, corresponding to the power of the damping function associated to the longest relaxation time, is lower for polyethylenes showing high nonlinear effects (i.e., high intensity of the third harmonic I_3/I_1) and is higher for linear macromolecular structures. Whereas the differential pompom model has allowed prediction of I_3/I_1 for all nine polymers, it was only able to predict the whole complex harmonic I^*_3/I_1 for six polymers showing the lowest nonlinear behaviors. For these six polymers, the macromolecular structure following from the pompom model has been correlated to the supposed structure expected from the type of synthesis and from classical viscoelastic measurements (such as zero-shear viscosity, Cole−Cole relaxation time, and van Gurp−Palmen plots). Thus, FTR seems to be an efficient method to predict the architecture of linear, sparsely, or densely branched polyethylene.

Acknowledgment. The authors wish to thank the Research laboratory of Feluy (Belgium) of Total Elf Fina for the PE samples and SEC experiments. The authors would also like to thank Dr. Manfred Wilhelm, Dr. C. Oelschlaeger and J. Vittorias from the Max Planck Institute of Mainz (Germany) for very useful discussions regarding FTR experiments and for complementary SEC measurements.

References and Notes

(1) Fujimoto, T.; Narukawa, H.; Nagasawa, M. *Macromolecules* **1970**, *3*, 57−64.
(2) Roovers, J. *Macromolecules* **1984**, *17*, 1196−1200.
(3) Daniels, D. R.; McLeish, T. C. B.; Crosby, B. J.; Young, R. N.; Fernyhough, C. M. *Macromolecules* **2001**, *34*, 7025−7033.
(4) Kaye, A. *The College of Aeronautics*; Cranfield, U.K., 1962; Note 134.
(5) Bernstein, B, Kearsley, E. A.; Zapas, L. J. *Trans. Soc. Rheol*. **1963**, *7*, 391−410.
(6) Wagner, M. H.; Laun, H. M. *Rheol. Acta* **1978**, *17*, 138−148.
(7) Wagner, M. H.; Raible, T.; Meissner, J. *Rheol. Acta* **1979**, *18*, 427−428.
(8) Baaijens, F. P. T.; Selen, S. H. A.; Baaijens, H. P. W.; Peters, G. W. M.; Meijer, H. E. H. *J. Non-Newtonian Fluid Mech.* **1997**, *68*, 173−203.
(9) Béraudo, C.; Fortin, A.; Coupez, T.; Demay, Y.; Vergnes, B.; Agassant, J. F. *J. Non-Newtonian Fluid Mech.* **1998**, *75*, 1−23.
(10) McLeish, T. C. B.; Larson, R. G. *J. Rheol.* **1998**, *42*, 81−110.
(11) McLeish, T. C. B.; Allgaier, J.; Bick, D. K.; Bishko, G.; Biswas, P.; Blackwell, R.; Blottiere, B.; Clarke, N.; Gibbs, B.; Groves, D. J.; Hakiki, A.; Heenan, R. K.; Johnson, J. M.; Kant, R.; Read, D. J.; Young, R. N. *Macromolecules* **1999**, *32*, 6734−6758.

(12) Inkson, N. J.; McLeish, T. C. B.; Harlen, O. G.; Groves, D. J. *J. Rheol.* **1999**, *43*, 873−896.
(13) Read, D. J.; McLeish, T. C. B. *Macromolecules* **2001**, *34*, 1928−1945.
(14) Blackwell, R. J.; Harlen, O. G.; McLeish, T. C. B. *Macromolecules* **2001**, *34*, 2579−2596.
(15) Groves, D. J.; McLeish, T. C. B.; Blackwell, R. J. *Proc. Int. Congr. Rheol. 13th* **2000**, *1*, 95−97.
(16) Vega, J. F.; Fernandez, M.; Santamaria, A.; Muñoz-Escalona, A.; Lafuente, P. *Macromol. Chem. Phys.* **1999**, *200*, 2257−2268.
(17) Yan, D.; Wang, W. J.; Zhu, S. *Polymer* **1999**, *40*, 1737−1744.
(18) Janzen, J.; Colby, R. H. *J. Mol. Struct.* **1999**, *486*, 569−584.
(19) Malmberg, A.; Kokko, E.; Lehmus, P.; Löfgren, B.; Seppälä, J. V. *Macromolecules* **1998**, *31*, 8448−8454.
(20) Malmberg, A.; Gabriel, C.; Löfgren, B.; Steffl, T. *Proc. Int. Congr. Rheol. 13th* **2000**, *1*, 174−176.
(21) Baird, D.; Bortner, M.; Doerpinghaus, P. *Proc. Int. Congr. Rheol. 13th* **2000**, *1*, 228−230.
(22) Trinkle, S.; Friedrich, C. *Rheol. Acta* **2001**, *40*, 322−328.
(23) Trinkle, S.; Walter, P.; Friedrich, C. *Rheol. Acta* **2002**, *41*, 103−113.
(24) van Gurp, M.; Palmen, J. *Rheol. Bull.* **1998**, *67*, 5−8.
(25) Garcia-Franco, C. A.; Srinivas, S.; Lohse, D. J.; Brant, P. *Macromolecules* **2001**, *34*, 3115−3117.
(26) Lohse, D. J.; Milner, S. T.; Fetters, L. J.; Xenidou, M.; Hadjichristidis, N.; Mendelson, R. A.; Garcia-Franco, C. A.; Lyon, M. K. *Macromolecules* **2002**, *35*, 3066−3075.
(27) Wood-Adams, P. M.; Dealy, J. M.; deGroot, A. W.; Redwine, O. D. *Macromolecules* **2000**, *33*, 7489−7499.
(28) Robertson, C. G.; Garcia-Franco, C. A.; Srinivas, S. *J. Polym. Sci., Part B: Polym. Phys.* **2004**, *42*, 1671−1684.
(29) Heinrich, M.; Pyckhout-Hintzen, W.; Allgaier, J.; Richter, D.; Straube, E.; Read, D. J.; McLeish, T. C. B.; Groves, D. J.; Blackwell, R. J.; Wiedenmann, A. *Macromolecules* **2002**, *35*, 6650−6664.
(30) Doerpinghaus, P. J.; Baird, D. G. *Macromolecules* **2002**, *35*, 10087−10095.
(31) MacSporran, W. C.; Spiers, R. P. *Rheol. Acta* **1982**, *21*, 184−200.
(32) MacSporran, W. C.; Spiers, R. P. *Rheol. Acta* **1984**, *23*, 90−96.
(33) Hyun, K.; Kim, S. H.; Ahn, K. H.; Lee, S. J. *J. Non-Newtonian Fluid Mech.* **2002**, *107*, 51−65.
(34) Wilhelm, M. *Macromol. Mater. Eng.* **2002**, *287*, 83−105.
(35) Wilhelm, M.; Maring, D.; Spiess, H. W. *Rheol. Acta* **1998**, *37*, 399−405.
(36) Wilhelm, M.; Reinheimer, P.; Ortseifer, M. *Rheol. Acta* **1999**, *38*, 349−356.
(37) Leblanc, J. L. *J. Appl. Polym. Sci.* **2003**, *89*, 1101−1115.
(38) Debbaut, B.; Burhin, H. *J. Rheol.* **2002**, *46*, 1155−1176.
(39) Clemeur, N.; Rutgers, R. P. G.; Debbaut, B. *Rheol. Acta* **2003**, *42*, 217−231.
(40) Fleury, G.; Schlatter, G.; Muller, R. *Rheol. Acta* **2004**, *44*, 174−187.
(41) Hamielec, A. E.; Soares, J. B. P. *Prog. Polym. Sci.* **1996**, *21*, 651−706.
(42) Mavridis, H.; Shroff, R. N. *Polym. Eng. Sci.* **1992**, *32*, 1778−1791.
(43) Giacommin, A. J.; Dealy, J. M. In *Techniques in Rheological Measurements*; Collyer, A. A., Ed.; Chapman and Hall: London, 1993; Chapter 4, p 99−121.
(44) Neidhöfer, T.; Wilhelm, M.; Debbaut, B. *J. Rheol.* **2003**, *47*, 1351−1371.
(45) Wagner, M. H.; Stephenson, S. E. *J. Rheol.* **1979**, *23*, 489−504.
(46) Larson, R. G. In *Constitutive Equations for Polymer Melts and Solutions*; Butterworth Publishers: Massachusetts, 1988.
(47) Khan, M. M. K.; Tanner, R. I. *Rheol. Acta* **1990**, *29*, 281−297.
(48) Lee, K.; Mackley, M. R.; McLeish, T. C. B.; Nicholson, T. M.; Harlen, O. G. *J. Rheol.* **2001**, *45*, 1261−1277.

MA0505530